Near-Field ISAC in Cluttered Environments via Partial Relaxation

Mohammad Abu Aqoulah[1,4], Doğa Gürgünoğlu[2], Gábor Fodor[3,4], Gonzalo Seco-Granados[1]
[1]Universitat Autònoma de Barcelona (UAB), CERES, Barcelona, Spain
[2]ASELSAN Inc., Ankara, Türkiye
[3]School of EECS, KTH Royal Institute of Technology, Stockholm, Sweden
[4]Ericsson Research, Stockholm, Sweden
Emails: {Mohammad.AbuAqoulah@uab.cat, dgurgunoglu@aselsan.com, gabor.fodor@ericsson.com, gonzalo.seco@uab.cat}

***Abstract*—Near-field integrated sensing and communication (ISAC) enables high-resolution sensing and wireless communication using a common platform and waveform. However, target localization in cluttered near-field environments remains challenging, particularly in bistatic architectures with separated communication and sensing receivers. In this paper, we investigate clutter-aware target localization for a bistatic near-field ISAC system. We first derive the Cramér–Rao bound (CRB) for target localization in clutter and use it as a benchmark. We then develop a partial-relaxation covariance-fitting framework that preserves the desired target component in structured form while modeling the aggregate undesired contribution as a relaxed nuisance term. Numerical results show that the proposed method achieves reliable localization in cluttered near-field conditions, outperforms conventional subspace-based baselines, and attains performance close to the CRB, while capturing a meaningful communication–sensing trade-off under a common transmit precoder.**

***Index Terms*—Bistatic ISAC, clutter, Cramér–Rao bound, near-field sensing, partial relaxation, target localization.**

I. Introduction

Integrated sensing and communication (ISAC) has emerged as a promising paradigm for future wireless systems, since it enables communication and sensing functionalities to share the same platform, hardware infrastructure, and transmitted waveform [1], [2]. In particular, near-field ISAC has attracted considerable attention due to its enhanced spatial resolution and richer location-dependent propagation structure. Unlike the conventional far-field regime, near-field propagation is governed by a spherical-wave model in which both angle and distance shape the array response, thereby improving localization capability [3].

Target localization in cluttered near-field environments remains challenging. In practical sensing scenarios, the received data contain not only the desired target return but also undesired reflections from surrounding scatterers and environmental clutter, which can obscure weak target returns and degrade localization accuracy [4]. The problem becomes even more involved in bistatic ISAC architectures with separated communication and sensing receivers, where the communication user receives the direct downlink signal while the sensing receiver observes only reflected echoes [3], [5]. Although near-field and passive sensing have been investigated in related ISAC settings, including multiple signal classification (MUSIC)-based localization approaches, these studies do not directly address clutter-aware target localization under the present bistatic communication-centric shared-waveform model [6].

Existing works on ISAC have made important progress in waveform design, sensing with communication signals, and high-resolution parameter estimation [1], [7], [8]. Recent communication-centric bistatic sensing studies have shown that useful sensing information can be extracted directly from communication transmissions [3]. In parallel, the partial-relaxation framework has emerged as an alternative to conventional spectral and subspace-based estimators by preserving the structure of the component of interest while relaxing the remaining interference contribution [9]. Recent near-field studies further indicate the suitability of partial-relaxation-based formulations for structured channel-parameter estimation under spherical-wave propagation [10], [11]. However, clutter-aware target localization in bistatic near-field ISAC remains insufficiently understood, especially when the near-field bistatic geometry, shared-waveform sensing mechanism, and clutter are jointly accounted for in a tractable formulation [4].

Motivated by these observations, this paper investigates clutter-aware target localization for a bistatic near-field ISAC architecture with separated communication and sensing receivers, where sensing is performed using the transmitted communication waveform itself. We derive the Cramér–Rao bound (CRB) for target localization in clutter as a benchmark and develop a sensing-side partial-relaxation covariance fitting (PR-CF) localization method that preserves the desired target covariance structure while representing the aggregate undesired covariance as a relaxed low-rank nuisance term. The proposed formulation is further restricted to a prescribed region of interest (ROI), consistent with coordinated infrastructure-based sensing. Numerical results demonstrate the effectiveness of the proposed method in cluttered near-field conditions and illustrate the resulting communication–sensing trade-off under a common transmit precoder.

This work has been partially supported by the European Union's Horizon Europe Marie Sklodowska-Curie Innovative Training Networks HORIZON-MSCA-2022-DN-01 call, under Grant Agreement "MiFuture" No. 101119643, by the Spanish Agency of Research (AEI) under grant PID2023-152820OB-I00, funded by MICIU/AEI/10.13039/501100011033 and ERDF/EU, and by the Catalan Government under the AGAUR-ICREA Academia Program. G. Fodor was also supported by the Swedish Strategic Research (SSF) grant for the FUS21-0004 SAICOM project.

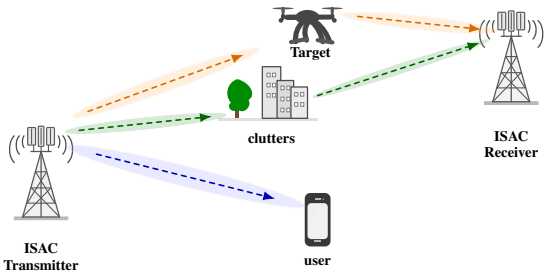


Fig. 1: Illustration of the considered bistatic near-field ISAC scenario.

II. Bistatic Near-Field ISAC System Model

We consider a bistatic near-field downlink ISAC system with separated communication and sensing receivers. A multi-antenna ISAC transmitter radiates a common waveform, the communication user receives the direct downlink signal, and a spatially separated sensing receiver collects the echoes reflected from the environment. The setup comprises one ISAC transmitter, one communication user, one sensing receiver, one desired target, and multiple clutter scatterers. Thus, communication and sensing are coupled through the same transmitted waveform while being observed at different nodes. The considered geometry is illustrated in Fig. 1.

a) Near-field geometry and bistatic channel model: The transmitter employs an N_t-element uniform linear array (ULA), and the sensing receiver employs an N_r-element ULA. Since the relevant propagation links lie in the radiative near-field region, the spatial responses depend on both angle and distance and are therefore described by a spherical-wave model rather than the conventional planar-wave approximation. For an array aperture D, the radiative near-field region is typically associated with propagation distances below the Rayleigh distance $2D^2/\lambda$, where λ is the carrier wavelength. Let $(x_{\mathrm{T}}, y_{\mathrm{T}})$ and $(x_{\mathrm{R}}, y_{\mathrm{R}})$ denote the reference-point coordinates of the transmit and receive arrays, respectively, and let d_t and d_r denote the corresponding inter-element spacings.

The coordinates of the n-th transmit element and the m-th receive element are

$$(x_{\mathrm{T},n}, y_{\mathrm{T},n}) = (x_{\mathrm{T}} + n d_t,\ y_{\mathrm{T}}), \quad n \in \mathcal{N}_t, \tag{1}$$

$$(x_{\mathrm{R},m}, y_{\mathrm{R},m}) = (x_{\mathrm{R}} + m d_r,\ y_{\mathrm{R}}), \quad m \in \mathcal{N}_r, \tag{2}$$

where $\mathcal{N}_t$ and $\mathcal{N}_r$ denote the centered antenna-index sets.

For a generic point (x, y), the distances from the transmit and receive reference points are

$$\begin{aligned} r_{\mathrm{T}}(x,y) &= \sqrt{(x_{\mathrm{T}} - x)^2 + (y_{\mathrm{T}} - y)^2}, \\ r_{\mathrm{R}}(x,y) &= \sqrt{(x_{\mathrm{R}} - x)^2 + (y_{\mathrm{R}} - y)^2}, \end{aligned} \tag{3}$$

while the distances from the n-th transmit element and the m-th receive element are

$$\begin{aligned} r_{\mathrm{T},n}(x,y) &= \sqrt{(x_{\mathrm{T}} + n d_t - x)^2 + (y_{\mathrm{T}} - y)^2}, \\ r_{\mathrm{R},m}(x,y) &= \sqrt{(x_{\mathrm{R}} + m d_r - x)^2 + (y_{\mathrm{R}} - y)^2}. \end{aligned} \tag{4}$$

The corresponding transmit-side and receive-side near-field response vectors, $\mathbf{a}_{\mathrm{T}}(x,y) \in \mathbb{C}^{N_t \times 1}$ and $\mathbf{a}_{\mathrm{R}}(x,y) \in \mathbb{C}^{N_r \times 1}$, are defined element-wise as

$$[\mathbf{a}_{\mathrm{T}}(x,y)]_n = e^{-j\frac{2\pi}{\lambda}(r_{\mathrm{T},n}(x,y) - r_{\mathrm{T}}(x,y))}, \quad n \in \mathcal{N}_t, \tag{5}$$

$$[\mathbf{a}_{\mathrm{R}}(x,y)]_m = e^{-j\frac{2\pi}{\lambda}(r_{\mathrm{R},m}(x,y) - r_{\mathrm{R}}(x,y))}, \quad m \in \mathcal{N}_r, \tag{6}$$

For a generic bistatic path associated with the point (x, y), let β denote the effective propagation coefficient. Following the standard bistatic propagation form in [3], it is given by

$$\beta = \sqrt{G_{\mathrm{T}}(x,y)\, G_{\mathrm{R}}(x,y)}\, \frac{\lambda \sqrt{\sigma^{\mathrm{bi}}(x,y)}}{(4\pi)^{3/2}\, r_{\mathrm{T}}(x,y)\, r_{\mathrm{R}}(x,y)} e^{j\delta(x,y)}, \tag{7}$$

where $G_{\mathrm{T}}(x,y)$ and $G_{\mathrm{R}}(x,y)$ denote the transmit- and receive-side gains, $\sigma^{\mathrm{bi}}(x,y)$ denotes the effective bistatic reflection strength, and $\delta(x,y)$ is the common phase term. The bistatic channel associated with (x,y) is then modeled as

$$\mathbf{G}(x,y) = \beta\, \mathbf{a}_{\mathrm{R}}(x,y)\, \mathbf{a}_{\mathrm{T}}^{T}(x,y). \tag{8}$$

Accordingly, the desired target and the q-th clutter channels are defined as $\mathbf{G}_t \triangleq \mathbf{G}(x_t, y_t)$ and $\mathbf{G}_{c,q} \triangleq \mathbf{G}(x_{c,q}, y_{c,q})$, respectively. Thus, the sensing-side channel structure is governed by the transmit and receive near-field manifolds, while the path-dependent effects are absorbed into the propagation coefficients.

b) Common transmitted signal and precoder: We adopt a shared-waveform transmission model in which the ISAC transmitter radiates a single communication waveform that is simultaneously used for sensing, following the communication-centric ISAC principle in [1]. The waveform is directly received by the communication user while also illuminating the environment and generating the target- and clutter-related echoes observed at the sensing receiver. Let $c[\ell] \in \mathbb{C}$ denote the communication symbol transmitted at snapshot ℓ. The transmitted signal is modeled as

$$\mathbf{x}[\ell] = \sqrt{P}\, \mathbf{w}(\rho)\, c[\ell] \in \mathbb{C}^{N_t \times 1}, \tag{9}$$

where $P \in \mathbb{R}_+$ denotes the total transmit power and $\mathbf{w}(\rho) \in \mathbb{C}^{N_t \times 1}$ denotes the common transmit precoder. To capture the communication–sensing trade-off induced by the shared waveform, the common precoder is parameterized as

$$\mathbf{w}(\rho) = \frac{\sqrt{\rho}\, \mathbf{w}_{\mathrm{c}} + \sqrt{1-\rho}\, \mathbf{w}_{\mathrm{s}}}{\left\| \sqrt{\rho}\, \mathbf{w}_{\mathrm{c}} + \sqrt{1-\rho}\, \mathbf{w}_{\mathrm{s}} \right\|_2}, \qquad 0 \le \rho \le 1, \tag{10}$$

where $\mathbf{w}_{\mathrm{c}}$ and $\mathbf{w}_{\mathrm{s}}$ denote the communication-oriented and sensing-oriented precoders, respectively. Hence, ρ controls the operating point of the common beam: larger values favor communication, whereas smaller values favor sensing.

c) Communication-side received signal model: For the communication branch, we adopt a standard single-user fading model. Let $\alpha_u \in \mathbb{R}_+$ denote the large-scale propagation coefficient of the communication link, and let $\mathbf{h}_u \in \mathbb{C}^{N_t \times 1}$ denote the small-scale channel vector between the ISAC transmitter and the communication user. The communication channel is modeled as Rayleigh fading according to

$$\mathbf{h}_u \sim \mathcal{CN}(\mathbf{0}, \mathbf{C}_u), \tag{11}$$

where $\mathbf{C}_u \in \mathbb{C}^{N_t \times N_t}$ denotes the channel covariance matrix. The received signal at the communication user at snapshot ℓ is then given by

$$y_u[\ell] = \alpha_u\, \mathbf{h}_u^{T} \mathbf{x}[\ell] + z_u[\ell], \tag{12}$$

where $z_u[\ell] \sim \mathcal{CN}(0, \sigma_u^2)$ denotes the additive communication noise. Substituting (9) into (12) yields

$$y_u[\ell] = \alpha_u \sqrt{P}\, \mathbf{h}_u^T \mathbf{w}(\rho)\, c[\ell] + z_u[\ell]. \tag{13}$$

Define the effective scalar communication channel as

$$g_u(\rho) \triangleq \alpha_u\, \mathbf{h}_u^T \mathbf{w}(\rho). \tag{14}$$

Then the communication-side received signal can be written in the compact form

$$y_u[\ell] = \sqrt{P}\, g_u(\rho)\, c[\ell] + z_u[\ell]. \tag{15}$$

In the subsequent communication-side model, the instantaneous realization of the effective channel is assumed to be known at the communication receiver. Accordingly, the effective communication signal-to-noise ratio is given by

$$\mathrm{SNR}_u(\rho) \triangleq \frac{P|g_u(\rho)|^2}{\sigma_u^2}, \tag{16}$$

and the corresponding instantaneous achievable rate is

$$R_u(\rho) \triangleq \log_2\!\left(1 + \frac{P|g_u(\rho)|^2}{\sigma_u^2}\right) = \log_2\!\big(1 + \mathrm{SNR}_u(\rho)\big). \tag{17}$$

d) Sensing-side received signal model: At the sensing receiver, the observed signal consists of the desired target return, the clutter returns, and additive noise. Since sensing is performed using the same transmitted communication waveform, each reflected component is generated by the transmitted signal impinging on a target or clutter scatterer and then propagating to the sensing receiver. Over L snapshots, define

$$\mathbf{X} \triangleq \begin{bmatrix} \mathbf{x}[1] & \mathbf{x}[2] & \cdots & \mathbf{x}[L] \end{bmatrix} \in \mathbb{C}^{N_t \times L},$$

$$\mathbf{Y}_r \triangleq \begin{bmatrix} \mathbf{y}_r[1] & \mathbf{y}_r[2] & \cdots & \mathbf{y}_r[L] \end{bmatrix} \in \mathbb{C}^{N_r \times L},$$

$$\mathbf{Z}_r \triangleq \begin{bmatrix} \mathbf{z}_r[1] & \mathbf{z}_r[2] & \cdots & \mathbf{z}_r[L] \end{bmatrix} \in \mathbb{C}^{N_r \times L},$$

where each noise vector satisfies $\mathbf{z}_r[\ell] \sim \mathcal{CN}(\mathbf{0}, \sigma_r^2 \mathbf{I}_{N_r})$. The sensing-side received signal model is then given by

$$\mathbf{Y}_r = \underbrace{\mathbf{G}_t \mathbf{X}}_{\text{desired target return}} + \underbrace{\sum_{q=1}^{M_c} \mathbf{G}_{c,q} \mathbf{X}}_{\text{clutter returns}} + \underbrace{\mathbf{Z}_r}_{\text{additive sensing noise}}. \tag{18}$$

In (18), the desired target contribution is structured by the receive-side near-field manifold $\mathbf{a}_{\mathrm{R}}(x_t, y_t)$, while its effective amplitude is determined by the target coefficient, the transmitted communication symbols, and the transmit-side illumination induced by the common precoder. The clutter term is modeled as the superposition of the reflected returns from the clutter scatterers. The main sensing parameter of interest is the target location

$$\boldsymbol{\eta}_t \triangleq \begin{bmatrix} x_t \\ y_t \end{bmatrix} \in \mathbb{R}^{2\times 1}, \tag{19}$$

which is estimated from the sensing-side observations in the presence of clutter.

III. Cramér–Rao Bound for Target Localization

To benchmark the achievable localization accuracy, we derive the CRB for estimating the desired target location under the considered bistatic near-field ISAC model. In the coordinated sensing setting considered here, the transmitted communication waveform is known at the sensing receiver and is therefore treated as deterministic. The benchmark accounts for the dominant clutter paths through their near-field geometric responses, while the associated complex reflection coefficients remain unknown and are treated as nuisance parameters. These nuisance parameters are included in the Fisher information matrix (FIM) and eliminated through the Schur complement, yielding the equivalent information bound for the target-location parameters.

a) Gaussian FIM: For a complex Gaussian observation vector, modeled as $\mathbf{y} \sim \mathcal{CN}(\mathbf{m}(\boldsymbol{\alpha}), \boldsymbol{\Gamma}(\boldsymbol{\alpha}))$, and under the adopted sensing model where the unknown parameters affect only the mean while the covariance is determined solely by the additive sensing noise, the (i,j)-th entry of the FIM is given by [12]

$$[\mathbf{F}_{\boldsymbol{\alpha}}]_{ij} = 2\Re\left\{ \frac{\partial \mathbf{m}^H}{\partial \alpha_i} \boldsymbol{\Gamma}^{-1} \frac{\partial \mathbf{m}}{\partial \alpha_j} \right\}. \tag{20}$$

b) Observation model for CRB derivation: Starting from the sensing-side matrix model in (18), define

$$\mathbf{b}_t(x_t, y_t) \triangleq \mathbf{X}^T \mathbf{a}_{\mathrm{T}}(x_t, y_t), \qquad \mathbf{b}_{c,q} \triangleq \mathbf{X}^T \mathbf{a}_{\mathrm{T}}(x_{c,q}, y_{c,q}),$$

so that

$$\mathbf{Y}_r = \beta_t \mathbf{a}_{\mathrm{R}}(x_t,y_t)\mathbf{b}_t^T(x_t,y_t) + \sum_{q=1}^{M_c} \beta_{c,q} \mathbf{a}_{\mathrm{R}}(x_{c,q},y_{c,q}) \mathbf{b}_{c,q}^T + \mathbf{Z}_r. \tag{21}$$

Vectorizing (21) and using $\mathrm{vec}(\mathbf{a}\mathbf{b}^T) = \mathbf{b} \otimes \mathbf{a}$ gives

$$\begin{aligned} \mathbf{y} \triangleq \mathrm{vec}(\mathbf{Y}_r) &= \beta_t \big(\mathbf{b}_t(x_t, y_t) \otimes \mathbf{a}_{\mathrm{R}}(x_t, y_t)\big) \\ &\quad + \sum_{q=1}^{M_c} \beta_{c,q} \big(\mathbf{b}_{c,q} \otimes \mathbf{a}_{\mathrm{R}}(x_{c,q}, y_{c,q})\big) + \bar{\mathbf{z}}_r, \end{aligned} \tag{22}$$

where $\bar{\mathbf{z}}_r \triangleq \mathrm{vec}(\mathbf{Z}_r) \sim \mathcal{CN}(\mathbf{0}, \sigma_r^2 \mathbf{I}_{N_r L})$. Hence, $\mathbf{y} \sim \mathcal{CN}(\mathbf{m}(\boldsymbol{\alpha}), \boldsymbol{\Gamma})$ with

$$\begin{aligned} \mathbf{m}(\boldsymbol{\alpha}) &= \beta_t \big(\mathbf{b}_t(x_t, y_t) \otimes \mathbf{a}_{\mathrm{R}}(x_t, y_t)\big) \\ &\quad + \sum_{q=1}^{M_c} \beta_{c,q} \big(\mathbf{b}_{c,q} \otimes \mathbf{a}_{\mathrm{R}}(x_{c,q}, y_{c,q})\big), \end{aligned} \tag{23}$$

and covariance $\boldsymbol{\Gamma} = \sigma_r^2 \mathbf{I}_{N_r L}$.

c) Unknown parameter vector: The parameters of interest are the target coordinates (x_t, y_t), while the target coefficient β_t and the clutter coefficients $\{\beta_{c,q}\}_{q=1}^{M_c}$ are treated as nuisance parameters. Writing

$$\beta_t = \beta_t^{(r)} + j\beta_t^{(i)}, \qquad \beta_{c,q} = \beta_{c,q}^{(r)} + j\beta_{c,q}^{(i)}, \quad q = 1, \ldots, M_c,$$

the real-valued parameter vector is defined as

$$\boldsymbol{\alpha} \triangleq \Big[\underbrace{x_t \;\; y_t}_{\text{target location}} \;\; \underbrace{\beta_t^{(r)} \;\; \beta_t^{(i)}}_{\text{target coefficient}} \;\; \underbrace{\boldsymbol{\beta}_c^T}_{\text{clutter coefficients}} \Big]^T \in \mathbb{R}^{(4+2M_c)\times 1}$$

where

$$\boldsymbol{\beta}_c \triangleq \begin{bmatrix} \beta_{c,1}^{(r)} & \beta_{c,1}^{(i)} & \cdots & \beta_{c,M_c}^{(r)} & \beta_{c,M_c}^{(i)} \end{bmatrix}^T.$$

d) Mean-vector derivatives: From (23), only the desired target term depends on the target-location parameters (x_t, y_t), while the clutter is treated through relaxed nuisance coefficients. Let $\mathbf{a}_{R,t} \triangleq \mathbf{a}_{\mathrm{R}}(x_t, y_t)$, $\mathbf{a}_{T,t} \triangleq \mathbf{a}_{\mathrm{T}}(x_t, y_t)$, $\mathbf{b}_t \triangleq \mathbf{X}^T\mathbf{a}_{T,t}$, $\mathbf{a}_{R,c,q} \triangleq \mathbf{a}_{\mathrm{R}}(x_{c,q}, y_{c,q})$, $\mathbf{a}_{T,c,q} \triangleq \mathbf{a}_{\mathrm{T}}(x_{c,q}, y_{c,q})$, and $\mathbf{b}_{c,q} \triangleq \mathbf{X}^T\mathbf{a}_{T,c,q}$. Hence,

$$\frac{\partial \mathbf{m}}{\partial x_t} = \beta_t \left(\frac{\partial \mathbf{b}_t}{\partial x_t} \otimes \mathbf{a}_{R,t} + \mathbf{b}_t \otimes \frac{\partial \mathbf{a}_{R,t}}{\partial x_t} \right), \tag{24}$$

$$\frac{\partial \mathbf{m}}{\partial y_t} = \beta_t \left(\frac{\partial \mathbf{b}_t}{\partial y_t} \otimes \mathbf{a}_{R,t} + \mathbf{b}_t \otimes \frac{\partial \mathbf{a}_{R,t}}{\partial y_t} \right), \tag{25}$$

where

$$\frac{\partial \mathbf{b}_t}{\partial x_t} = \mathbf{X}^T \frac{\partial \mathbf{a}_{T,t}}{\partial x_t}, \qquad \frac{\partial \mathbf{b}_t}{\partial y_t} = \mathbf{X}^T \frac{\partial \mathbf{a}_{T,t}}{\partial y_t}. \tag{26}$$

The derivatives with respect to the real and imaginary parts of the target coefficient are

$$\frac{\partial \mathbf{m}}{\partial \beta_t^{(r)}} = \mathbf{b}_t \otimes \mathbf{a}_{R,t}, \qquad \frac{\partial \mathbf{m}}{\partial \beta_t^{(i)}} = j\,\mathbf{b}_t \otimes \mathbf{a}_{R,t}, \tag{27}$$

and, for each clutter component,

$$\frac{\partial \mathbf{m}}{\partial \beta_{c,q}^{(r)}} = \mathbf{b}_{c,q} \otimes \mathbf{a}_{R,c,q}, \qquad \frac{\partial \mathbf{m}}{\partial \beta_{c,q}^{(i)}} = j\,\mathbf{b}_{c,q} \otimes \mathbf{a}_{R,c,q}, \tag{28}$$

e) Near-field steering-vector derivatives: Using the element-wise steering-vector definitions in (5) and (6), let $\mathbf{a}_\kappa \triangleq \mathbf{a}_\kappa(x, y)$ denote a generic near-field steering vector, where $\kappa \in \{\mathrm{T}, \mathrm{R}\}$ denotes the transmit or receive side. Then, for its i-th entry,

$$\frac{\partial [\mathbf{a}_\kappa]_i}{\partial x} = [\mathbf{a}_\kappa]_i \left(-j\frac{2\pi}{\lambda} \right) \left(\frac{x - (x_\kappa + id_\kappa)}{r_{\kappa,i}(x,y)} - \frac{x - x_\kappa}{r_\kappa(x,y)} \right),$$

$$\frac{\partial [\mathbf{a}_\kappa]_i}{\partial y} = [\mathbf{a}_\kappa]_i \left(-j\frac{2\pi}{\lambda} \right) \left(\frac{y - y_\kappa}{r_{\kappa,i}(x,y)} - \frac{y - y_\kappa}{r_\kappa(x,y)} \right),$$

where $\kappa = \mathrm{T}$ and $\kappa = \mathrm{R}$ correspond to the transmit-side and receive-side derivatives, respectively.

f) FIM construction and CRB: Using the derivatives in (24)–(28), the FIM is obtained from (20). Since $\boldsymbol{\Gamma} = \sigma_r^2 \mathbf{I}_{N_r L}$, the resulting FIM follows directly, where the derivative matrix $\mathbf{D}$ collects the mean-vector derivatives with respect to all entries of $\boldsymbol{\alpha}$. Partitioning the parameter vector as $\boldsymbol{\alpha} = [\boldsymbol{\eta}_t^T \ \boldsymbol{\nu}^T]^T$, with $\boldsymbol{\eta}_t = [x_t \ y_t]^T$ and $\boldsymbol{\nu}$ collecting the nuisance parameters, the equivalent Fisher information matrix for the target location is obtained through the Schur complement as $\mathbf{J}_\eta = \mathbf{F}_{\eta\eta} - \mathbf{F}_{\eta\nu}\mathbf{F}_{\nu\nu}^{-1}\mathbf{F}_{\nu\eta}$, and the corresponding CRB matrix is $\mathbf{C}_\eta = \mathbf{J}_\eta^{-1}$. Accordingly,

$$\mathrm{CRB}_{x_t} = [\mathbf{C}_\eta]_{1,1}, \qquad \mathrm{CRB}_{y_t} = [\mathbf{C}_\eta]_{2,2}, \tag{29}$$

and the scalar localization benchmark is

$$\mathrm{CRB}_{\mathrm{loc}} \triangleq \sqrt{[\mathbf{C}_\eta]_{1,1} + [\mathbf{C}_\eta]_{2,2}}. \tag{30}$$

IV. Partial-Relaxation-Based Target Localization

We develop a sensing-side target-localization method based on partial-relaxation covariance fitting (PR-CF), where the desired target component is preserved in structured form while the aggregate undesired contribution is represented through a relaxed nuisance term [9]. The formulation is tailored to the considered bistatic near-field ISAC setting with shared-waveform sensing and is restricted to a prescribed sensing region of interest (ROI) $\mathcal{R}_{\mathrm{ROI}} \subset \mathbb{R}^2$, within which the desired target is searched for and the remaining reflections are treated as nuisance components.

a) Signal- and covariance-domain formulation: The proposed sensing method is formulated in the covariance domain. To make the partial-relaxation structure explicit, we separate the sensing-side received signal in (18) into the desired target contribution and the aggregate undesired term by defining

$$\mathbf{Y}_t \triangleq \mathbf{G}_t\mathbf{X}, \qquad \mathbf{Y}_u \triangleq \sum_{q=1}^{M_c} \mathbf{G}_{c,q}\mathbf{X} + \mathbf{Z}_r. \tag{31}$$

For a candidate target location $(x_t, y_t) \in \mathcal{R}_{\mathrm{ROI}}$, the target covariance is modeled in structured form as

$$\mathbf{R}_t(x_t, y_t) = p_t\, \mathbf{a}_{\mathrm{R}}(x_t, y_t)\mathbf{a}_{\mathrm{R}}^H(x_t, y_t), \qquad p_t \geq 0, \tag{32}$$

where the effective scalar weight p_t absorbs the transmit-side response, common precoder, and communication symbols. Defining the sensing covariance and aggregate undesired covariance as $\mathbf{R}_r \triangleq \mathbb{E}[\mathbf{y}_r[\ell]\mathbf{y}_r^H[\ell]]$ and $\mathbf{R}_u \triangleq \mathbb{E}[\mathbf{y}_u[\ell]\mathbf{y}_u^H[\ell]]$, respectively, we obtain

$$\mathbf{R}_r = \mathbf{R}_t(x_t, y_t) + \mathbf{R}_u. \tag{33}$$

Following the partial-relaxation principle, the undesired covariance is represented through the relaxed low-rank factorization $\mathbf{R}_u = \mathbf{E}_c\mathbf{E}_c^H$, with $\mathbf{E}_c \in \mathbb{C}^{N_r \times M_c}$. Therefore,

$$\mathbf{R}_r = p_t\, \mathbf{a}_{\mathrm{R}}(x_t, y_t)\mathbf{a}_{\mathrm{R}}^H(x_t, y_t) + \mathbf{E}_c\mathbf{E}_c^H. \tag{34}$$

In practice, $\mathbf{R}_r$ is replaced by the sample covariance matrix

$$\widehat{\mathbf{R}}_r \triangleq \frac{1}{L}\mathbf{Y}_r\mathbf{Y}_r^H. \tag{35}$$

b) PR-CF optimization problem: Based on (34), the sensing-side localization problem is formulated as

$$\begin{aligned} \underset{(x_t,y_t)\in\mathcal{R}_{\mathrm{ROI}},\, p_t,\, \mathbf{E}_c}{\text{minimize}} \quad & \left\| \widehat{\mathbf{R}}_r - p_t\, \mathbf{a}_{\mathrm{R}}(x_t, y_t)\mathbf{a}_{\mathrm{R}}^H(x_t, y_t) - \mathbf{E}_c\mathbf{E}_c^H \right\|_F^2 \\ \text{subject to} \quad & p_t \geq 0, \qquad \mathrm{rank}(\mathbf{E}_c) \leq M_c. \end{aligned} \tag{36}$$

c) Elimination of the relaxed nuisance covariance and target weight.: For fixed (x_t, y_t) and p_t, let $\mathbf{a}_t \triangleq \mathbf{a}_{\mathrm{R}}(x_t, y_t)$ and define the residual covariance

$$\mathbf{S}_r(x_t, y_t, p_t) \triangleq \widehat{\mathbf{R}}_r - p_t\, \mathbf{a}_t\mathbf{a}_t^H. \tag{37}$$

Then (36) reduces to a best rank-M_c positive-semidefinite approximation problem for $\mathbf{S}_r(x_t, y_t, p_t)$. Let

$$\mathbf{S}_r = \mathbf{U}_r\, \mathrm{diag}(\lambda_1, \ldots, \lambda_{N_r})\, \mathbf{U}_r^H, \qquad \lambda_1 \geq \lambda_2 \geq \cdots \geq \lambda_{N_r}, \tag{38}$$

be its eigendecomposition. The resulting concentrated PR-CF cost is

$$f_{\text{PR-CF}}(x_t, y_t, p_t) = \sum_{k=M_c+1}^{N_r} \lambda_k^2\big(\mathbf{S}_r(x_t, y_t, p_t)\big). \tag{39}$$

For fixed (x_t, y_t), the target covariance weight is profiled using a constrained covariance-fitting step. Following the covariance-fitting interpretation of the Capon spectrum [9], we enforce the residual covariance condition $\widehat{\mathbf{R}}_r - p_t \mathbf{a}_t \mathbf{a}_t^H \succeq \mathbf{0}$. Under this condition, the largest admissible target weight, attained at the positive-semidefinite boundary, is given by

$$p_t^\star(x_t, y_t) = \frac{1}{\mathbf{a}_t^H \widehat{\mathbf{R}}_r^{-1} \mathbf{a}_t}. \tag{40}$$

This Capon-type profiling provides a stable normalization of the structured target component before fitting the remaining relaxed nuisance covariance. Substituting (40) into (37) gives

$$\mathbf{S}_r^\star(x_t, y_t) \triangleq \widehat{\mathbf{R}}_r - \frac{\mathbf{a}_t \mathbf{a}_t^H}{\mathbf{a}_t^H \widehat{\mathbf{R}}_r^{-1} \mathbf{a}_t}. \tag{41}$$

Hence, the final concentrated cost is

$$\bar{f}_{\text{PR-CF}}(x_t, y_t) = \sum_{k=M_c+1}^{N_r} \lambda_k^2\big(\mathbf{S}_r^\star(x_t, y_t)\big), \tag{42}$$

and the target-location estimate is obtained as

$$(\widehat{x}_t, \widehat{y}_t) = \arg \min_{(x_t, y_t) \in \mathcal{R}_{\text{ROI}}} \bar{f}_{\text{PR-CF}}(x_t, y_t). \tag{43}$$

d) Near-field MUSIC baseline: As a sensing-side baseline, we consider near-field MUSIC at the sensing receiver. The eigendecomposition of the sensing-side sample covariance matrix is used to construct the noise subspace $\mathbf{U}_{n,r}$. For MUSIC, the signal-subspace dimension is set to $M_c + 1$, corresponding to one desired target and M_c dominant clutter components. Using the receive-side near-field steering vector $\mathbf{a}_{\text{R}}(x, y)$, the corresponding MUSIC pseudo-spectrum is given by

$$P_{\text{MUSIC}}(x, y) \triangleq \frac{1}{\mathbf{a}_{\text{R}}^H(x, y)\, \mathbf{U}_{n,r} \mathbf{U}_{n,r}^H\, \mathbf{a}_{\text{R}}(x, y)}. \tag{44}$$

The MUSIC estimate is

$$(\widehat{x}_t, \widehat{y}_t)_{\text{MUSIC}} = \arg \max_{x,y} P_{\text{MUSIC}}(x, y). \tag{45}$$

V. Numerical Results

This section evaluates the proposed bistatic near-field ISAC localization framework through four complementary results. We first study the communication–sensing trade-off under the common precoder and identify a suitable operating point. We then fix the target at the nominal precoding center $(20, 10)$ m and examine how the sensing-side localization performance varies with signal-to-clutter-plus-noise ratio (SCNR) and with the number of snapshots. We finally move the target within the ROI to quantify the localization degradation caused by transmit-beam mismatch away from the precoding center.

TABLE I: Simulation parameters

Parameter	Fig. 2	Fig. 3	Fig. 4	Fig. 5
Precoder parameter (ρ)	0.1–0.9	0.55	0.55	0.55
SCNR	2–18	0–30 dB	20 dB	20 dB
Snapshots (L)	10	10	10–10000	10
Carrier frequency (f_c)	3 GHz			
Antenna numbers (N_t, N_r)	34, 34			
Number of clutter scatterers (M_c)	4			
TX location (x_T, y_T)	(10,0) m			
RX location (x_R, y_R)	(0,40) m			
ROI	$x \in [15, 25]$ m, $y \in [5, 15]$ m			

a) Simulation setup: The simulations follow the system model in Section II, and the adopted parameters are summarized in Table I. Here, $f_c = 3$ GHz with half-wavelength antenna spacing, yielding $R_{\text{NF}} \approx 54.5$ m; hence, the considered geometry lies in the near-field range.The sensing SCNR is defined as $P_{\text{tar}}/(P_{\text{cl}} + P_{\text{n}})$, where P_{tar}, P_{cl}, and P_{n} denote the received target, clutter, and noise powers, respectively. The sensing-side performance is evaluated through the localization root-mean-squared error (RMSE), computed over $N_{\text{MC}} = 1000$ Monte Carlo realizations as

$$\text{RMSE}_{\text{loc}} = \sqrt{\frac{1}{N_{\text{MC}}} \sum_{n=1}^{N_{\text{MC}}} \Big[(\widehat{x}_t^{(n)} - x_t)^2 + (\widehat{y}_t^{(n)} - y_t)^2\Big]}.$$

b) Results: We begin with the communication–sensing trade-off in Fig. 2, which shows how the common precoder parameter ρ shifts the operating point between communication and sensing. As ρ increases, the achievable communication rate improves, while the sensing-side localization RMSE produced by the proposed PR-CF method in Section IV degrades. The corresponding CRB benchmark is computed from Section III. From this curve, $\rho = 0.55$ is selected as a representative knee point that balances communication-rate improvement and sensing-RMSE degradation.

After fixing $\rho = 0.55$, we place the target at the nominal precoding center $(20, 10)$ m and study sensing performance under aligned illumination. Figure 3 shows the localization RMSE versus SCNR for fixed L. As SCNR increases, the localization error decreases. The proposed PR-CF method outperforms MUSIC and remains close to the CRB, even in the presence of clutter and limited snapshot support. Figure 4 shows the localization RMSE versus L for fixed SCNR. As L increases, the covariance estimate becomes more accurate, which improves localization performance. In this case, PR-CF approaches the CRB from about $L = 500$ onward and remains superior to the MUSIC baseline throughout. When $L < N_r$, the sample covariance matrix becomes singular, so diagonal loading is applied as $\widehat{\mathbf{R}}_r \leftarrow \widehat{\mathbf{R}}_r + \rho_{\text{dl}} \mathbf{I}$, with $\rho_{\text{dl}} = 10^{-4}$.

We finally assess the sensitivity of the sensing performance to the target location by fixing $\rho = 0.55$, fixing SCNR and L, and moving the target across the ROI while keeping the common precoder directed toward the same precoding center. The heatmap in Fig. 5 shows that the localization performance is strongest near the illumination center and degrades as the target moves away from it, especially near the ROI boundaries, due to transmit-beam mismatch. This result highlights the spatial dependence of the sensing performance under fixed illumination across the prescribed sensing region.

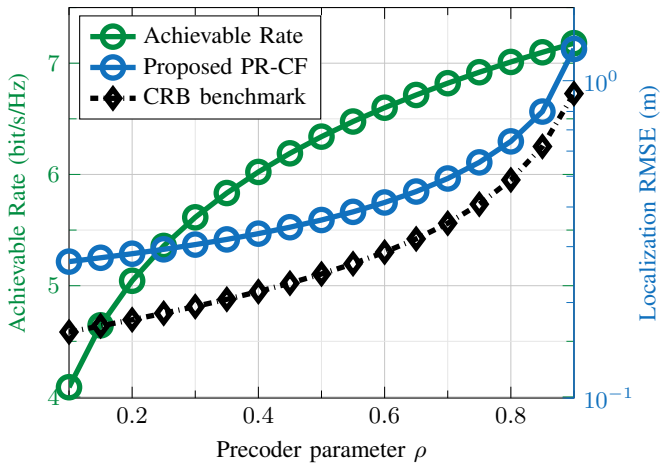


Fig. 2: Communication–sensing trade-off under the common precoder parameter ρ at $L = 10$.

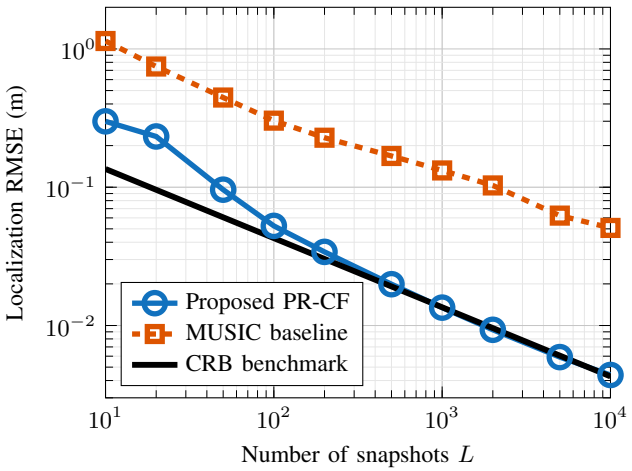


Fig. 4: Localization RMSE versus the number of snapshots at $\rho = 0.55$ and SCNR $= 20$ dB.

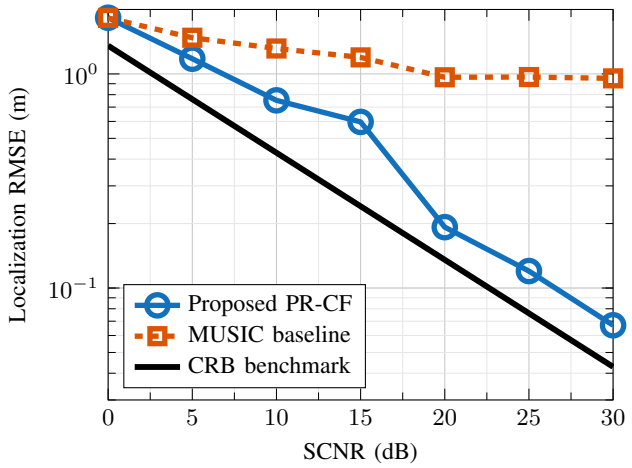


Fig. 3: Localization RMSE versus SCNR at $\rho = 0.55$ and $L = 10$.

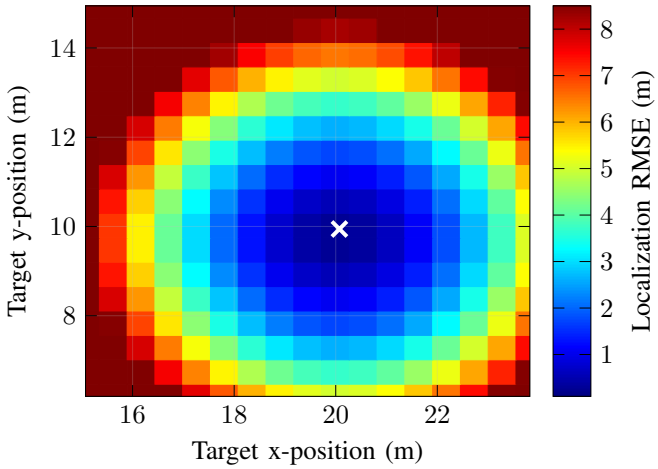


Fig. 5: Localization RMSE over the ROI under fixed precoding-center illumination at $\rho = 0.55$, SCNR $= 20$ dB, and $L = 10$. The white marker denotes the nominal precoding center $(20, 10)$ m.

VI. Conclusion

This paper investigated clutter-aware target localization for a bistatic near-field ISAC system with separated communication and sensing receivers under a shared-waveform transmission model. A sensing-side CRB was derived as a benchmark, and a PR-CF localization method was developed by preserving the desired target covariance while relaxing the aggregate undesired contribution. Numerical results showed that the proposed method provides reliable localization in clutter, consistently outperforms MUSIC, and approaches the CRB as the snapshot support increases. The results also demonstrated the expected communication–sensing trade-off and the effect of spatial illumination mismatch over the sensing region.

References

[1] F. Liu *et al.*, "Sensing with communication signals: From information theory to signal processing," *IEEE J. Sel. Areas Commun*, vol. 44, pp. 1–30, 2026.

[2] Y. Lyazidi *et al.*, "ISAC architecture for 6G cellular networks with sensing topology switching," *IEEE Communications Standards Magazine*, pp. 1–7, 2025.

[3] S. Naoumi *et al.*, "High-resolution sensing in communication-centric ISAC: Deep learning and parametric methods," *IEEE J. Sel. Areas Commun*, vol. 44, pp. 2201–2216, 2026.

[4] R. Liu *et al.*, "Clutter-aware integrated sensing and communication: Models, methods, and future directions," *Proc. IEEE*, pp. 1–41, 2026.

[5] S. Fodor *et al.*, "Bistatic integrated sensing and communication scenarios with transmitter and receiver-side trade-offs," in *Proc. IEEE 5th Int. Symp. Joint Commun. Sens. (JC&S)*, 2025, pp. 1–6.

[6] J. Chen *et al.*, "Passive sensing in a near-field multi-ISAC system with imperfect CSI," *IEEE Trans. Cogn. Commun. Netw*, vol. 12, pp. 4186–4197, 2026.

[7] S. Fodor, G. Fodor, and M. Telek, "On the trade-off between angle of arrival and symbol estimation in bistatic ISAC systems using unitary signaling," *IEEE Trans. Comm.*, vol. 73, no. 7, pp. 5328–5343, 2025.

[8] S. Daei *et al.*, "Near-field ISAC in 6G: Addressing phase nonlinearity via lifted super-resolution," in *IEEE Int. Conference on Acoustics, Speech and Signal Processing (ICASSP)*, 2025, pp. 1–5.

[9] M. Trinh-Hoang, M. Viberg, and M. Pesavento, "Partial relaxation approach: An eigenvalue-based DoA estimator framework," *IEEE Trans. Signal Process*, vol. 66, no. 23, pp. 6190–6203, 2018.

[10] M. A. Aqoulah *et al.*, "Partial relaxation for near-field channel parameter estimation: Algorithms and Cramér–Rao bounds," in *Proc. IEEE ICC Workshops*, 2026.

[11] M. A. Aqoulah *et al.*, "Low-complexity multi-user non-line-of-sight channel estimation," 2026, accepted for publication in IEEE CSCN 2026. [Online]. Available: https://arxiv.org/abs/2609.29342

[12] S. M. Kay, *Fundamentals of Statistical Signal Processing, Volume I: Estimation Theory*. Englewood Cliffs, NJ, USA: Prentice-Hall, 1993.